

# Recently measured large $A_N$ for forward neutrons in $p^\uparrow A$ collisions at $\sqrt{s_{NN}} = 200$ GeV explained through simulations of ultraperipheral collisions and hadronic interactions

Gaku Mitsuka

RIKEN BNL Research Center, Brookhaven National Laboratory, Upton, New York 11973-5000, USA  
(Dated: February 20, 2017)

The PHENIX experiment at the Relativistic Heavy Ion Collider recently reported that transverse single spin asymmetry,  $A_N$ , for forward neutrons in  $p^\uparrow A$  collisions at  $\sqrt{s_{NN}} = 200$  GeV.  $A_N$  in  $p^\uparrow \text{Al}$  and  $p^\uparrow \text{Au}$  collisions were measured as  $-0.015$  and  $0.18$ , respectively. These values are clearly different from the measured  $A_N = -0.08$  in  $p^\uparrow p$  collisions. In this paper, we propose that a large  $A_N$  for forward neutrons in ultraperipheral  $p^\uparrow A$  collisions may explain the PHENIX measurements. The proposed model is demonstrated using two Monte Carlo simulations. In the ultraperipheral collision simulation, we use the STARLIGHT event generator for the simulation of the virtual photon flux and then use the MAID2007 unitary isobar model for the simulation of the neutron production in the interactions of a virtual photon with a polarized proton. In the  $p^\uparrow A$  hadronic interaction simulation, the differential cross sections for forward neutron production are predicted by a simple one-pion exchange model and the Glauber model. The simulated  $A_N$  values for both the contribution of ultraperipheral collisions and the hadronic interactions are in good agreement with the PHENIX results.

PACS numbers: 13.85.-t, 13.85.Tp, 24.85.+p

## I. INTRODUCTION

The PHENIX experiment at the Relativistic Heavy Ion Collider (RHIC) reported that the transverse single spin asymmetry, denoted  $A_N$ , for forward neutrons measured in transversely polarized proton–nucleus ( $p^\uparrow A$ ) collisions at  $\sqrt{s_{NN}} = 200$  GeV is far different from that in polarized proton–proton ( $p^\uparrow p$ ) collisions at  $\sqrt{s} = 200$  GeV [1]. That is, the measured  $A_N$  for  $p^\uparrow \text{Al}$  and  $p^\uparrow \text{Au}$  collisions are  $-0.015 \pm 0.005$  and  $0.18 \pm 0.03$ , respectively. On the other hand,  $A_N$  is  $-0.08 \pm 0.02$  in  $p^\uparrow p$  collisions [2]. In these measurements, the neutrons produced in  $p^\uparrow p$  and  $p^\uparrow A$  collisions are detected by a zero-degree calorimeter [3] in the polarized proton remnant side that is defined as the positive rapidity region.

As studied in Ref. [4], the interference of pion (spin-flip) and  $a_1$ -Reggeon (spin nonflip) exchanges successfully explains  $A_N$  for forward neutrons in  $p^\uparrow p$  collisions at RHIC. We would expect that this mechanism can be extended to predict  $A_N$  for  $p^\uparrow A$  collisions. The authors of Ref. [4] incorporate the pion– $a_1$ -Reggeon interference with strong nuclear absorptive corrections and a nuclear breakup [5]. However, the predicted  $A_N$  in  $p^\uparrow A$  collisions remains negative and the magnitude of  $A_N$  is too small to explain the PHENIX results.

In this paper, we propose an alternative mechanism: ultraperipheral proton–nucleus collisions (UPCs) [6, 7]. UPCs occur when the impact parameter  $b$  is larger than the sum of the radii of each colliding particle, namely,  $b > R_p + R_A$ , where  $R_p$  and  $R_A$  are the radius of the proton and nucleus, respectively. As we explored in Ref. [8], UPCs have a comparable cross section with the hadronic interactions in the very forward rapidity region. In ultraperipheral  $p^\uparrow A$  collisions, virtual photons ( $\gamma^*$ ) emitted from the relativistic nucleus interact with polarized protons. Thus the number of neutrons produced via the  $\gamma^* p^\uparrow$

interaction depends on the azimuthal angle of the scattered neutrons relative to the proton polarization. This may finally contribute to the large  $A_N$  for forward neutrons in  $p^\uparrow A$  collisions.

We first develop the Monte Carlo (MC) simulation framework for UPCs (Sec. II) and hadronic interactions (Sec. III). In Sec. IV, using these MC simulations we show that UPCs in  $p^\uparrow A$  collisions have sizable cross sections compared with hadronic interactions and the yield of forward neutrons in UPCs certainly depend on the scattering azimuthal angle relative to the proton polarization axis. Finally, in Sec. V, we compare the simulated  $A_N$  with the PHENIX results. Conclusions are drawn in Sec. VI. Natural units  $\hbar = c = 1$  are used throughout.

## II. METHODOLOGY OF ULTRAPERIPHERAL COLLISIONS MONTE CARLO SIMULATIONS

The MC simulation for UPCs in this study comprises two steps. First, we simulate the virtual photon flux as a function of the photon energy and impact parameter by using STARLIGHT [9, 10] (Sec. II B). Second, the simulation of the  $\gamma^* p^\uparrow$  interaction and particle production is performed following the differential cross sections that are predicted by the MAID2007 model [11] (Sec. II C).

### A. Formalism for ultraperipheral $p^\uparrow A$ collisions

The differential cross section for single neutron production in  $p^\uparrow A$  UPCs is given by

$$\frac{d\sigma_{\text{UPC}(p^\uparrow A \rightarrow \pi^+ n)}^4}{dW db^2 d\Omega_n} = \frac{d^3 N_{\gamma^*}}{dW db^2} \frac{d\sigma_{\gamma^* p^\uparrow \rightarrow \pi^+ n}(W)}{d\Omega_n} \overline{P}_{\text{had}}(b) \quad (1)$$

where  $N_{\gamma^*}$  is the number of the emitted photons,  $W$  is the  $\gamma^*p^\dagger$  center-of-mass energy,  $d\Omega_n = \sin\theta_n d\theta_n d\phi_n$  with the neutron scattering polar angle  $\theta_n$  and azimuthal angle  $\phi_n$  in the  $\gamma^*p^\dagger$  center-of-mass frame,  $\sigma_{\gamma^*p^\dagger \rightarrow \pi^+n}(W)$  is the total cross section for a single photon interaction with a proton leading to single neutron production, and  $\overline{P_{\text{had}}}(b)$  is the probability of having no hadronic interactions in  $p^\dagger A$  collisions at given  $b$ . We calculate  $d^3N_{\gamma^*}/dW db^2$  and  $d\sigma_{\gamma^*p^\dagger \rightarrow \pi^+n}(W)/d\Omega_n$  in Sec. II B and Sec. II C, respectively.

A finite probability for having no hadronic interactions  $\overline{P_{\text{had}}}(b)$  is introduced in order to account for a smooth cut off around the impact parameter  $b = R_p + R_A$  [9].  $R_p$  and  $R_A$ , where  $R_{\text{Al}} \sim 5$  fm and  $R_{\text{Au}} \sim 7$  fm, are the radius of the proton and nucleus, respectively. The range of the impact parameter considered in the simulation extends from  $b_{\text{min}} = 4$  fm to  $b_{\text{max}} = 10^5$  fm. The value of  $b_{\text{min}}$  is well below the sum of the effective radii of colliding particles, and  $\overline{P_{\text{had}}}(b)$  rapidly approaches zero below these nuclear radii.

For comparisons with the simulation results of hadronic interactions in Sec. IV and the experimental results from PHENIX in Sec. V, we will numerically transform the differential cross section in Eq. (1) based on the  $\gamma^*p^\dagger$  center-of-mass frame to that in the detector reference frame. Both frames are defined in Fig. 1.

### B. Simulation of the virtual photon flux

For simplicity (unless otherwise noted), the discussion in this subsection is based on the proton rest frame. The virtual photons flux emitted by the relativistic nucleus is simulated using STARLIGHT, which follows the Weizsäcker-Williams approximation [12, 13]. The double differential photon flux due to the fast moving nucleus with velocity  $\beta$  is written as

$$\frac{d^3N_{\gamma^*}}{d\omega_{\gamma^*}^{\text{rest}} db^2} = \frac{Z^2 \alpha}{\pi^2} \frac{x^2}{\omega_{\gamma^*}^{\text{rest}} b^2} \left( K_1^2(x) + \frac{1}{\gamma^2} K_0^2(x) \right), \quad (2)$$

where  $\omega_{\gamma^*}^{\text{rest}}$  is the photon energy,  $Z$  is the atomic number ( $Z = 13$  and  $79$  for Al and Au, respectively),  $\alpha$  is the fine structure constant,  $x = \omega_{\gamma^*}^{\text{rest}} b / \gamma$  ( $\gamma = \sqrt{1 - \beta^2}^{-1/2}$  is the Lorentz factor), and  $K_0$  and  $K_1$  are the modified Bessel functions. In the case of a relativistic nucleus ( $\gamma \gg 1$ ), we safely disregard the contribution of the term  $K_0^2(x)/\gamma^2$  in Eq. (2). The photon energy  $\omega_{\gamma^*}^{\text{rest}}$  in the proton rest frame is properly transformed to the  $\gamma^*p^\dagger$  center-of-mass energy  $W$  to allow substitution of Eq. (2) for Eq. (1).

### C. Simulation of the $\gamma^*p^\dagger$ interaction

The kinematics of the  $\gamma^*p^\dagger$  interaction is shown in Fig. 1(b) and is defined as

$$\gamma^*(k) + p^\dagger(p) \rightarrow \pi^+(q) + n(n), \quad (3)$$

where the variables in brackets indicate the four-momenta of each particle. We use the following notations for these four-momenta:

$$\begin{aligned} k^\mu &= (\omega_{\gamma^*}, k), \\ p^\mu &= (\omega_p, -k), \\ q^\mu &= (\omega_\pi, q), \\ n^\mu &= (\omega_n, -q), \end{aligned} \quad (4)$$

where the  $\gamma^*p^\dagger$  center-of-mass energy is given by  $W = \omega_{\gamma^*} + \omega_{p^\dagger}$ .

Figure 1(b) also introduces the polar angle  $\theta_\pi$  and azimuthal angle  $\phi_\pi$  of  $\pi$ , with reference to a coordinate system with  $k$ , 1, and 2 axes such that  $k$  lies in the 1-3 plane. The proton is transversely polarized along the 2 axis. The frame  $\{1, 2, 3\}$  is the scattering plane. The frame  $\{x, y, z\}$  is defined such that the  $z$  axis is directed into the  $k$  direction; the  $y$  axis is perpendicular to the  $x$ - $z$  reaction plane; and the  $x$  axis is given by  $x = y \times z$ .

Single neutron and pion production from the  $\gamma^*p^\dagger$  interaction are simulated following the differential cross sections predicted by the MAID2007 model. The cross section of the  $\gamma^*p^\dagger \rightarrow \pi^+n$  interaction is formed as in Ref. [14]:

$$\begin{aligned} \frac{d\sigma_{\gamma^*p^\dagger \rightarrow \pi^+n}}{d\Omega_\pi} &= \frac{|q|}{\omega_{\gamma^*}} (R_T^{00} + P_y R_T^{0y}) \\ &= \frac{|q|}{\omega_{\gamma^*}} R_T^{00} (1 + P_2 \cos \phi_\pi T(\theta_\pi)), \end{aligned} \quad (5)$$

where  $R_T^{00}$  and  $R_T^{0y}$  are the response functions for pion photoproduction, and  $P_y$  and  $P_2$  are the proton polarization along  $y$  and 2 axes, respectively. In the third equation,  $R_T^{0y}/R_T^{00}$  and  $P_y$  respectively are replaced with target asymmetry  $T(\theta_\pi)$  and  $P_2 \cos \phi_\pi$ . We assume  $P_2 = 1$  and  $P_1 = 0$  in this study. Note that we can numerically obtain  $d\sigma_{\gamma^*p^\dagger \rightarrow \pi^+n}/d\Omega_\pi$  in Eq. (1) from  $d\sigma_{\gamma^*p^\dagger \rightarrow \pi^+n}/d\Omega_\pi$  in Eq. (5) with the relation  $\theta_n = \pi - \theta_\pi$  and  $\phi_n = \pi - \phi_\pi$ .

The photon virtuality is limited by  $Q^2 < (1/R_A)^2$ , thus  $Q^2 < 2 \times 10^{-3} \text{ GeV}^2$  in  $p^\dagger \text{Al}$  collisions and  $Q^2 < 6 \times 10^{-4} \text{ GeV}^2$  in  $p^\dagger \text{Au}$  collisions. In the following simulations, we fix  $Q^2 = 0 \text{ GeV}^2$  as default and take into account effects of nonzero  $Q^2$  as a model uncertainty. The virtual photons are assumed to be fully unpolarized in this study.

Both baryon resonance and nonresonance contributions are taken into account for neutron and pion productions in MAID2007. The model contains all four-star resonances with masses below 2 GeV and follows the Breit-Wigner forms for the resonance shape. Nonresonance background contribution contains the Born terms as detailed in Ref. [11].

Due to the energy range guaranteed by MAID2007, the minimum and maximum  $W$  values in the UPC MC simulation are set as  $W_{\text{min}} = 1.1 \text{ GeV}$  and  $W_{\text{max}} = 2.0 \text{ GeV}$ , respectively. We will discuss cross section contribution from outside the above energy range in Sec. IV A.

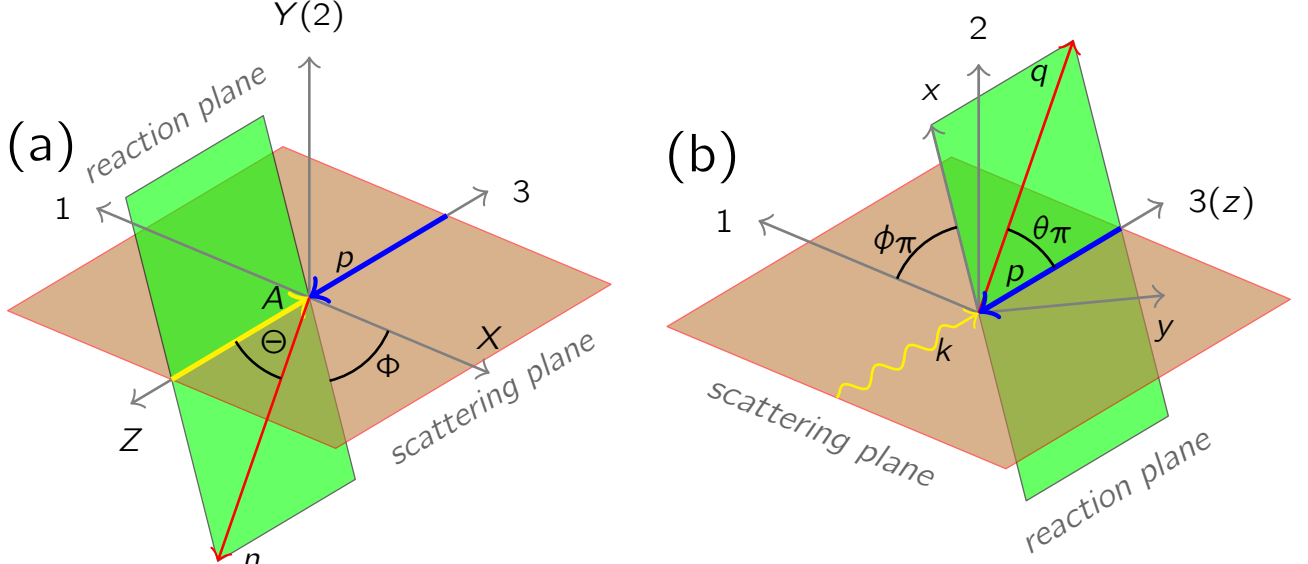


FIG. 1. (a) coordinate axes in the detector reference frame. (b) kinematical variables and coordinate axes in the  $\gamma^* p^\uparrow$  center-of-mass frame  $\{0, 2, 3\}$ .

Figure 2 shows  $T(\theta_\pi)$  of the  $\gamma^* p^\uparrow \rightarrow \pi^+ n$  interaction as a function of  $W$ . In the detector reference frame, the thick and thin curves correspond to the rapidity of produced neutrons of  $\eta = 6.8$  and  $8.0$ , respectively. Because the neutrons produced along the negative  $z$  axis, namely,  $\theta_\pi \sim 0$ , are more likely to have large positive rapidity in the detector reference frame, the thick and thin curves shift to the large  $\theta_\pi$  region.

### III. METHODOLOGY OF SIMULATIONS IN HADRONIC INTERACTIONS

Throughout this section, we use the detector reference frame defined in Fig. 1(a). We effectively obtain the differential cross section of forward neutron production in  $p^\uparrow A$  hadronic interactions as follows. First (Sec. III A), we calculate the cross section of inclusive neutrons in  $pp$  collisions,  $\sigma_{pp \rightarrow nX}$ , using a simple one-pion exchange model. Note that this calculation is performed for unpolarized protons. The one-pion exchange model has well described forward neutron production in  $pp$  collisions at the Intersecting Storage Rings [15] and RHIC [2] and in  $ep$  collisions at the Hadron-Electron Ring Accelerator (HERA) [16].

Second (Sec. III B), the cross section of the  $pA \rightarrow nX$  interaction,  $\sigma_{pA \rightarrow nX}$ , can be calculated by  $\sigma_{pp \rightarrow nX}$  and the Gribov-Glauber model [17, 18]. Here we avoid an implementation of multiple scattering of a projectile proton with a nucleus, and instead we multiply the  $pp$  cross section  $\sigma_{pp \rightarrow nX}$  with the inelastic cross section ratio  $\sigma_{pA}/\sigma_{pp}$  obtained from Ref. [19].

For the  $\Phi$ -dependence of the differential cross section,

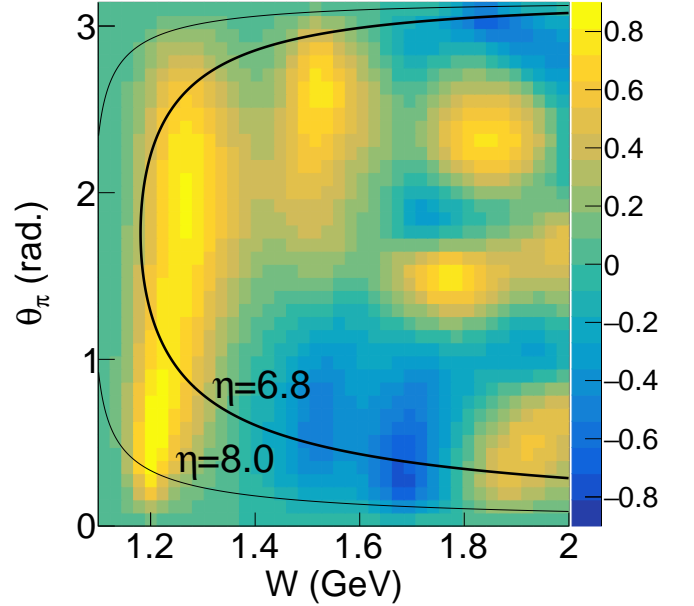


FIG. 2. Target asymmetry  $T(\theta_\pi)$  of the  $\gamma^* p^\uparrow \rightarrow \pi^+ n$  interaction as function of  $W$ . In the detector reference frame, the thick and thin curves correspond to the rapidity of produced neutrons  $\eta = 6.8$  and  $8.0$ , respectively.

we multiply  $d\sigma_{pA \rightarrow nX}/d\Omega_n$  with  $1 + \cos \Phi A_N^{\text{HAD}(pA)}$  in order to effectively take into account the single spin asymmetry  $A_N^{\text{HAD}(pA)}$  (Sec. III B).

### A. Simulation of the $pp$ interaction

The differential cross section for inclusive neutrons in  $pp$  collisions at the center-of-mass energy  $\sqrt{s}$  as a function of the longitudinal momentum fraction  $x_F$  and the transverse momentum  $p_T$  is formed in terms of the pion-exchange model [20] as

$$x_F \frac{d\sigma_{pp \rightarrow nX}}{dx_F dp_T^2} = S^2 \left( \frac{\alpha'_\pi}{8} \right)^2 |t| G_{\pi^+pn}^2(t) |\eta_\pi(t)|^2 \times (1 - x_F)^{1-2\alpha_\pi(t)} \sigma_{\pi^+p}^{\text{tot}}(M_X^2), \quad (6)$$

where  $S^2$  is the rapidity gap survival factor,  $\alpha_\pi = \alpha'_\pi(t - m_\pi^2)$  is the pion trajectory with the slope  $\alpha'_\pi$  and the pion mass  $m_\pi$ ,  $t$  is the four-momentum transfer squared,  $G_{\pi^+pn}(t)$  is the effective vertex function,  $\eta_\pi(t)$  is the phase factor [20], and  $\sigma_{\pi^+p}^{\text{tot}}(M_X^2)$  is the total cross section of the  $\pi^+p \rightarrow X$  interactions at the  $\pi^+p$  center-of-mass energy  $M_X^2 = (1 - x_F)s$ . The effective vertex function is parameterized as  $G_{\pi^+pn}(t) = g_{\pi^+pn} e^{R_\pi^2 t}$  using the pion-nucleon coupling  $g_{\pi^+pn}$  and the  $t$ -slope parameter  $R_\pi^2$ . In this study, we fix  $\alpha'_\pi = 1.0 \text{ GeV}^{-2}$  and  $g_{\pi^+pn}^2/8\pi = 13.75$  which are consistent with the results at HERA [16, 21], and follow the best COMPETE fit results [22] for  $\sigma_{\pi^+p}^{\text{tot}}(M_X^2)$ . Because the parameters  $S^2$  and  $R_\pi^2$  have been poorly determined to date, we use  $S^2 = 0.2$  and  $R_\pi^2 = 0.3 \text{ GeV}^{-2}$  that derive the best agreement with the forward neutron  $d\sigma_{p^\dagger p \rightarrow nX}/dx_F$  distribution measured at the PHENIX experiment [2]. These best-fit values are compatible with other experimental results [23].

### B. Single spin asymmetry in $p^\dagger A$ collisions

As introduced in the third paragraph of Sec. III, we avoid an implementation of multiple scattering of a projectile proton with a nucleus. On the other hand, we effectively obtain the  $pA$  cross sections  $\sigma_{pA \rightarrow nX}$  by multiplying  $\sigma_{pp \rightarrow nX}$  in Eq. (6) with the inelastic cross section ratio  $\sigma_{pA}/\sigma_{pp} = A^{0.42}$  that is calculated in Ref. [19]. Thus we obtain:

$$x_F \frac{d\sigma_{pA \rightarrow nX}}{dx_F dp_T^2} = x_F \frac{d\sigma_{pp \rightarrow nX}}{dx_F dp_T^2} A^{0.42}. \quad (7)$$

The single spin asymmetry for forward neutrons in  $p^\dagger p$  interactions originate in the interference of pion (spin-flip) and  $a_1$ -Reggeon (spin nonflip) exchanges [4] that well reproduces the result from the PHENIX experiment:  $A_N^{pp} = -0.08 \pm 0.02$  [2]. Preliminary results in Ref. [5] based on the same approach as Ref. [4] state that single spin asymmetry for forward neutrons in hadronic  $p^\dagger A$  collisions is also described by the pion- $a_1$ -Reggeon interference followed by a nuclear breakup. Here, we do not implement the pion- $a_1$  interference in the simulation. Instead, we multiply the  $pA$  differential cross section in Eq. (7) by  $1 + \cos \Phi A_N^{\text{HAD}(pA)}$ , where we

take  $A_N^{\text{HAD}(pAu)} = -0.05$  and  $A_N^{\text{HAD}(pAl)} = -0.05$  from Ref. [5].

Finally, we obtain using Eq. (7):

$$\begin{aligned} x_F \frac{d\sigma_{p^\dagger A \rightarrow nX}}{dx_F dp_T^2} &= x_F \frac{d\sigma_{pA \rightarrow nX}}{dx_F dp_T^2} (1 + \cos \Phi A_N^{\text{HAD}(pA)}) \\ &= x_F \frac{d\sigma_{pp \rightarrow nX}}{dx_F dp_T^2} A^{0.42} \\ &\quad \times (1 + \cos \Phi A_N^{\text{HAD}(pA)}). \end{aligned} \quad (8)$$

## IV. RESULTS

### A. Simulation results in $p^\dagger \text{Au}$ collisions at $\sqrt{s_{NN}} = 200 \text{ GeV}$

#### 1. The total cross sections

First, we calculate the total cross section of the  $p^\dagger \text{Au} \rightarrow nX$  interaction at  $\sqrt{s_{NN}} = 200 \text{ GeV}$  and compare it with UPCs and hadronic interactions. The total cross section for UPCs is calculated by integrating Eq. (1) over  $W$ ,  $b$ , and  $\Omega_n$ :

$$\begin{aligned} \sigma_{\text{UPC}(p^\dagger \text{Au} \rightarrow \pi^+ n)} &= \int_{\Omega_n} \int_{b_{\min}}^{b_{\max}} \int_{W_{\min}}^{W_{\max}} \frac{d\sigma_{\text{UPC}(p^\dagger \text{Au} \rightarrow \pi^+ n)}^4}{dW db^2 d\Omega_n} \\ &\quad \times \overline{P_{\text{had}}}(b) 2\pi b dW db d\Omega_n, \end{aligned} \quad (9)$$

where we require a single neutron scattered at  $y > 6.9$  and  $x_F > 0.4$ . The rapidity limit corresponds to the acceptance of a zero-degree calorimeter at RHIC and the  $x_F$  limit is introduced to remove the contribution of low-energy forward neutrons. These cuts are consistent with the RHIC measurements [2]. As addressed in Sec. II A, we fix  $b_{\min} = 4 \text{ fm}$ ,  $b_{\max} = 10^5 \text{ fm}$ ,  $W_{\min} = 1.1 \text{ GeV}$ , and  $W_{\max} = 2.0 \text{ GeV}$ . We then obtain  $\sigma_{\text{UPC}(p^\dagger \text{Au} \rightarrow \pi^+ n)} = 19.6 \text{ mb}$ .

For the discussions in Sec. IV A 2 and IV A 4, here we show the differential UPC cross sections at  $\sqrt{s_{NN}} = 200 \text{ GeV}$  as a function of  $W$  in Fig. 3. The  $d\sigma_{\text{UPC}(p^\dagger \text{Au})}/dW$  values are calculated by integrating Eq. (1) over  $b$  and  $\Omega_n$ . For simplicity, no kinematical limit is applied to such integration. Thick black curve indicates the  $p^\dagger \text{Au} \rightarrow \pi^+ n$  interaction and thin blue curve indicates the two-pion production  $\gamma^* p^\dagger \rightarrow \pi^+ \pi^0 n$ .

The total cross section for hadronic interaction is calculated by integrating Eq. (8) over  $x_F$  and  $p_T$ :

$$\sigma_{\text{HAD}(p^\dagger \text{Au} \rightarrow nX)} = 2\pi \int_{x_F} \int_{p_T} \frac{d\sigma_{p^\dagger \text{Au} \rightarrow nX}}{dx_F dp_T^2} p_T dp_T dx_F. \quad (10)$$

We obtain  $\sigma_{\text{HAD}(p^\dagger \text{Au} \rightarrow nX)} = 19.2 \text{ mb}$  by requiring a single neutron emitted into  $y > 6.9$  and  $x_F > 0.4$ . According to the comparison of these two cross sections, we find that UPCs lead to significant background contribution to the investigations of single spin asymmetry in terms of hadronic interactions. Table I summarizes the calculated cross sections.

TABLE I. Cross sections for neutron production in ultra-peripheral collisions and hadronic interactions at  $\sqrt{s_{NN}} = 200$  GeV. Cross sections in parentheses are calculated without  $\eta$  and  $x_F$  limits.

UPCs		Hadronic interactions	
$p^\dagger\text{Al}$	$p^\dagger\text{Au}$	$p^\dagger\text{Al}$	$p^\dagger\text{Au}$
0.7 mb (2.2 mb)	19.6 mb (41.7 mb)	8.3 mb	19.2 mb

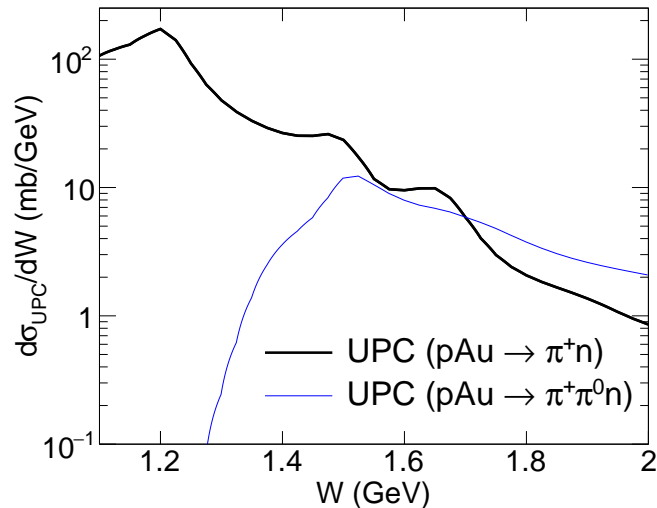


FIG. 3. The differential UPC cross sections as a function of  $W$ . Thick black curve indicates the  $p^\dagger\text{Au} \rightarrow \pi^+n$  interaction and thin blue curve indicates the  $p^\dagger\text{Au} \rightarrow \pi^+\pi^0n$  interaction.

## 2. The differential cross sections as a function of $x_F$

In Fig. 4(a), we show the differential cross sections as a function of  $x_F$ , namely,  $d\sigma/dx_F$ , for UPCs (dashed [red] line) and hadronic interactions (solid [black] line). UPCs dominate in  $d\sigma/dx_F$  at  $x_F > 0.6$  and have a sharp peak around  $x_F = 0.95$ . This peak originates from the  $\gamma^*p^\dagger \rightarrow \Delta^+(1232) \rightarrow \pi^+n$  channel in UPCs. As found in the thick black curve in Fig. 3, a  $\gamma^*p^\dagger$  center-of-mass energy of  $1.1 < W < 1.3$  GeV, a photon energy ranging from  $0.17 < \omega_{\gamma^*}^{\text{rest}} < 0.5$  GeV in the proton rest frame, corresponds to the  $\Delta^+(1232)$  baryon-resonance region that has a larger UPC cross section compared to higher energy regions due to the both ample photon flux and large  $\gamma^*p^\dagger \rightarrow \Delta^+(1232)$  cross section. Thus, low momentum neutrons produced by a pronounced  $\gamma^*p^\dagger$  interaction at  $1.1 < W < 1.3$  GeV and emitted into  $\theta_n \sim \pi$  in the  $\gamma^*p^\dagger$  center-of-mass frame are boosted to nearly the same velocity of the projectile proton in the detector reference frame. These neutrons lead to the forward neutrons sharply distributed around  $x_F = 0.95$ . Similarly, the neutrons emitted into  $\theta_n \sim 0$  at  $1.1 < W < 1.3$  GeV in the  $\gamma^*p^\dagger$  center-of-mass frame cause the second peak around  $x_F = 0.65$ .

## 3. The differential cross sections as a function of $\Phi$

In Fig. 4(b), we compare the differential cross section as a function of  $\Phi$ , namely,  $d\sigma/d\Phi$  between UPCs (dashed [red] line) and hadronic interactions (solid [black] line). We find that  $d\sigma/d\Phi$  of UPCs has substantial positive asymmetry  $A_N^{\text{UPC}(p\text{Au})}$  of about 0.36 compared with the negative asymmetry of hadronic interactions  $A_N^{\text{HAD}(p\text{Au})} = -0.05$ .

The UPC-induced asymmetry can be understood as follows. Replacing  $\phi_\pi$  with  $\Phi$  and  $P_2 = 1$  in Eq. (5), the  $\Phi$ -dependence of the differential UPC cross section is approximated as

$$\frac{d\sigma_{\text{UPC}}}{d\Phi} \propto 1 + \cos \Phi \langle T(\theta_\pi) \rangle, \quad (11)$$

where  $\langle T(\theta_\pi) \rangle$  is an average of  $T(\theta_\pi)$  over  $\theta_\pi$  but the rapidity and  $x_F$  limits,  $\eta < 6.8$  and  $x_F > 0.4$ , are applied. As we find in the  $d\sigma_{\text{UPC}(p^\dagger\text{Au})}/dW$  distribution in Fig. 3, forward neutrons in UPCs are mainly produced by the  $\Delta^+(1232) \rightarrow \pi^+n$  decay at  $1.1 < W < 1.3$  GeV, where  $\langle T(\theta_\pi) \rangle$  is  $\sim 0.7$ , as shown in Fig. 2. Conversely, resonances at  $1.4 < W < 1.8$  GeV have negative  $\langle T(\theta_\pi) \rangle$  below  $\theta_\pi \sim 0.5$ . Therefore  $d\sigma_{\text{UPC}}/d\Phi$  integrating over  $W$  suffers from the both positive and negative  $\langle T(\theta_\pi) \rangle$  and then we obtain  $\langle T(\theta_\pi) \rangle = 0.36$  at  $1.1 < W < 2.0$  GeV. In accordance with an equivalence  $A_N^{\text{UPC}(pA)} = \langle T(\theta_\pi) \rangle$ , we finally obtain  $A_N^{\text{UPC}(p\text{Au})} = 0.36$ .

## 4. Model uncertainties

Finally, we discuss the following three uncertainties in the present UPC cross sections: (1) the contribution from outside  $1.1 < W < 2.0$  GeV, (2) the contribution from the two-pion production process, and (3) the effects of nonzero  $Q^2$ .

(1) We first compare the UPC cross sections in the following three energy ranges:  $W < 1.1$  GeV,  $1.1 < W < 2.0$  GeV, and  $W > 2.0$  GeV. For the calculation of UPC cross sections, we use the framework in Ref. [8] instead of the framework developed in this paper, because MAID2007 provides the  $\gamma^*p^\dagger$  differential cross sections only at  $1.1 < W < 2.0$  GeV. In the framework in Ref. [8], the proton polarization is not taken into account, however the cross sections integrated over polar and azimuthal angles are independent of the target polarization. Unlike the framework developed in this paper, the total  $\gamma^*p^\dagger$  cross section  $\sigma_{\gamma^*p^\dagger \rightarrow \pi^+n}(W)$  in Ref. [8] is taken from the compilation of present experimental results [22] at  $W < 7$  GeV and from the best COMPETE fit results [22] at  $W > 7$  GeV. The UPC cross sections in each energy range are summarized in Table. II. Note that the rapidity and  $x_F$  limits,  $\eta > 6.9$  and  $x_F > 0.4$ , are applied to the these cross sections. According to Table II, we find that the cross sections at  $W < 1.1$  GeV

TABLE II. Cross sections in ultraperipheral  $p$ Au collisions at  $\sqrt{s_{NN}} = 200$  GeV.

$p\text{Au} \rightarrow nX$ ( $\eta > 6.9$ and $x_F > 0.4$ )			$p^\dagger\text{Au} \rightarrow \pi^+\pi^0n$
$< 1.1$ GeV	1.1–2.0 GeV	$> 2.0$ GeV	1.25–2.0 GeV
0.6 mb	27.4 mb	1.8 mb	6.2 mb

TABLE III. Summary of uncertainties in the UPC MC simulation.

(1) Energy range	$\sigma_{<1.1 \text{ GeV}}/\sigma_{1.1-2.0 \text{ GeV}}$	2.1 %
	$\sigma_{>2.0 \text{ GeV}}/\sigma_{1.1-2.0 \text{ GeV}}$	6.6 %
(2) Two-pion production	$\sigma_{p^\dagger\text{Au} \rightarrow \pi^+\pi^0n}/\sigma_{p^\dagger\text{Au} \rightarrow \pi^+n}$	14 %
(3) $Q^2$ range	$\sigma_{Q^2 \neq 0}/\sigma_{Q^2=0}$	$< 2$ %
	$A_N^{Q^2 \neq 0}/A_N^{Q^2=0}$	$-10$ %

and  $W > 2.0$  GeV are 2.1 % and 6.6 % of the cross section at  $1.1 < W < 2.0$  GeV, respectively.

(2) The contribution of the two-pion production  $\gamma^*p^\dagger \rightarrow \pi^+\pi^0n$  appears above the threshold energy  $W \approx 1.25$  GeV. The UPC cross section in Table II is calculated using the 2-PION MAID model [24], where the  $\eta$  and  $x_F$  limits are not applied to neutrons. Comparing UPCs leading to two-pion production, 6.2 mb present in Table II, with those leading to single pion production, 41.7 mb present in Table I, the former amounts to 14 % to the latter cross section. According to the discussions in (1) and (2), we find that UPCs at  $1.1 < W < 2.0$  GeV leading to single neutron and pion production dominantly contribute to the single spin asymmetry for neutrons.

(3) Effects of nonzero  $Q^2$  to single spin asymmetry in UPCs are tested by comparing the total cross sections and  $d\sigma/d\Phi$  distributions between  $Q^2 = 0$  and  $Q^2 \neq 0$ . For the nonzero  $Q^2$  values, we use  $Q^2 = 6 \times 10^{-4}$  GeV<sup>2</sup> in  $p^\dagger\text{Au}$  collisions and  $Q^2 = 2 \times 10^{-3}$  GeV<sup>2</sup> in  $p^\dagger\text{Al}$  collisions. In both collisions, the cross section for forward neutron production at  $Q^2 \neq 0$  is at most 2 % larger than those at  $Q^2 = 0$ . Because  $d\sigma/d\Phi$  is proportional to  $1 + P_2 \cos \Phi T(\theta_\pi)$  and  $T(\theta_\pi)$  is a function of  $Q^2$ , the  $d\sigma/d\Phi$  distribution is modified by  $Q^2$  depending on  $\cos \Phi$ . Accordingly,  $A_N^{\text{UPC}(p\text{Au})}$ , obtained from  $\langle T(\theta_\pi) \rangle$  averaged over  $W$  and  $\theta_\pi$ , at  $Q^2 = 1 \times 10^{-3}$  GeV<sup>2</sup> is  $\sim 10$  % smaller than that at  $Q^2 = 0$ .

The model uncertainties discussed in this subsection are summarized in Table III.

### B. Simulation results in $p^\dagger\text{Al}$ collisions at $\sqrt{s} = 200$ GeV

Total cross sections for UPCs and hadronic interactions in  $p^\dagger\text{Al}$  collisions are summarized in Table I. The UPC cross section is  $\sigma_{\text{UPC}(p^\dagger\text{Al})} = 0.7$  mb which is  $\sim 8$  % of  $\sigma_{\text{HAD}(p^\dagger\text{Al})} = 8.3$  mb, where UPCs in  $p^\dagger\text{Al}$  collisions are highly suppressed compared with those in  $p^\dagger\text{Au}$  collisions due to  $\propto Z^2$ .

Figure 4(c) shows  $d\sigma/dx_F$  for UPCs (dashed [red] line) and hadronic interactions (solid [black] line). We find UPCs leading to subdominant contribution to the  $d\sigma/dx_F$  distribution at  $x_F < 0.95$ .

Finally, Fig. 4(d) compares  $d\sigma/d\Phi$  between UPCs (dashed [red] line) and hadronic interactions (solid [black] line). Although the UPC cross section is about 8 % of the hadronic-interactions cross section, the large positive asymmetry of UPCs eventually compensates the small negative asymmetry of hadronic interactions.

## V. DISCUSSIONS

We compare the simulation results with the observed  $A_N$  values in  $p^\dagger\text{Al}$  and  $p^\dagger\text{Au}$  collisions at  $\sqrt{s_{NN}} = 200$  GeV. Figure 5 shows  $A_N$  as a function of the atomic number  $Z$  in  $p^\dagger p$  (for reference),  $p^\dagger\text{Al}$  and  $p^\dagger\text{Au}$  collisions.

Filled [black] circles indicate the  $A_N$  values inclusively measured by the PHENIX zero-degree calorimeter [1], where the neutron rapidity and  $x_F$  ranges are limited by  $6.8 < \eta < 8.8$  and  $x_F > 0.4$ , respectively. These values can be compared with open [red] circles indicating the sum of UPCs and hadronic interactions MC simulations, denoted  $A_N^{\text{UPC+HAD}}$ . These are written as

$$A_N^{\text{UPC+HAD}} = \frac{\sigma_{\text{UPC}} A_N^{\text{UPC}} + \sigma_{\text{HAD}} A_N^{\text{HAD}}}{\sigma_{\text{UPC}} + \sigma_{\text{HAD}}}, \quad (12)$$

since

$$\frac{d\sigma_{\text{UPC}}}{d\Phi} + \frac{d\sigma_{\text{HAD}}}{d\Phi} \propto 1 + \cos \Phi A_N^{\text{UPC+HAD}}. \quad (13)$$

For the MC simulation results (open [red] circles and open [blue] squares), the neutron rapidity and  $x_F$  region limits,  $6.8 < \eta < 8.8$  and  $x_F > 0.4$ , are also taken into account to be consistent with the PHENIX measurements. In  $p^\dagger\text{Al}$  collisions, we obtain  $A_N^{\text{UPC+HAD}} = -0.02$  which is consistent with the PHENIX result  $A_N = -0.015 \pm 0.005$ . In  $p^\dagger\text{Au}$  collisions, we have  $A_N^{\text{UPC+HAD}} = 0.16$  that can be understood by that UPCs, having large positive  $A_N^{\text{UPC}}$  and a cross section  $\sigma_{\text{UPC}} \approx \sigma_{\text{HAD}}$ , significantly contribute to the inclusive  $A_N^{\text{UPC+HAD}}$  value that are evident in Fig. 4 and Table I. Note that a model uncertainty in  $A_N^{\text{UPC+HAD}}$ , estimated by taking account of nonzero  $Q^2$  discussed in Sec. IV A 4, amounts 10 %.

Filled [black] squares in Fig. 5 are the  $A_N$  values measured by the PHENIX zero-degree calorimeter requiring a veto on the beam-beam counters (BBCs) covering  $3.0 < |\eta| < 3.9$  [25]. Because a nucleus in UPCs coherently scatters with a proton and thus does not generate underlying particles, such a BBC veto effectively selects UPC-rich events. In  $p^\dagger\text{Au}$  collisions, the PHENIX data with the BBC veto has larger  $A_N$  than the inclusive PHENIX data (filled [black] circle). This indicates that the fraction of UPCs in the PHENIX data is enhanced at a certain level by the BBC veto, although the actual fraction is not presently reported. Conversely in  $p^\dagger\text{Al}$

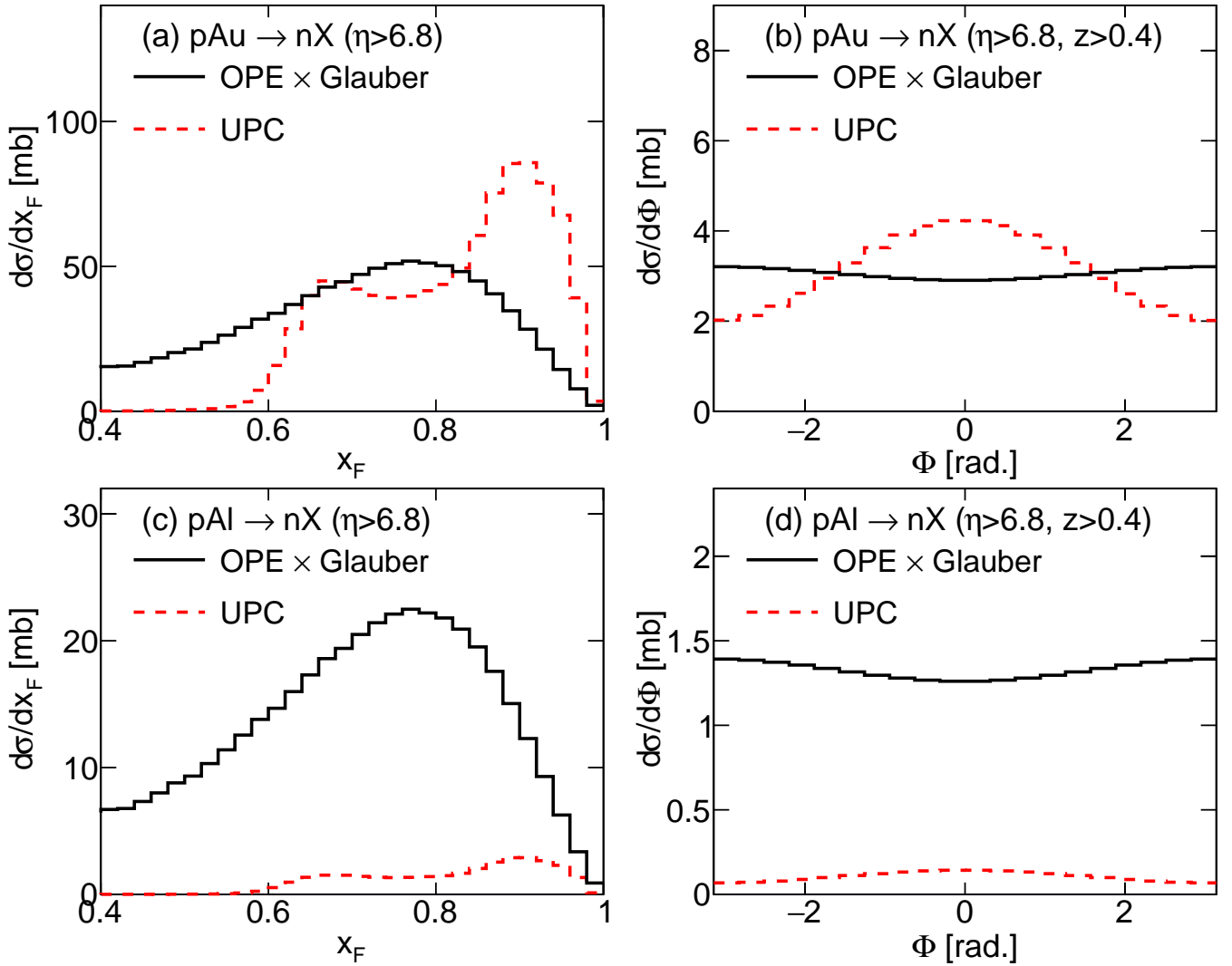


FIG. 4. The differential cross sections of UPCs and hadronic interactions as a function of  $x_F$  and  $\Phi$ . Solid [black] lines indicate hadronic interactions and dashed [red] lines indicate UPCs.

collisions, the PHENIX data with the BBC veto provides  $A_N = 0.085$  which is far smaller than  $A_N = 0.27 \pm 0.03$  in  $p^\uparrow Au$  collisions. A possible inference for the difference is that the fraction of hadronic interaction is still sizable in the PHENIX data in  $p^\uparrow Al$  collisions even though UPC-rich events are preferentially selected by the BBC veto. If pure UPC data is experimentally available, the  $A_N$  values may approach  $A_N^{\text{UPC}}$  in both  $p^\uparrow Al$  and  $p^\uparrow Au$  collisions. Note that  $A_N^{\text{UPC}}$  is same between  $p^\uparrow Al$  and  $p^\uparrow Au$  collisions, since  $A_N^{\text{UPC}}$  depends only on the  $\gamma^* p^\uparrow$  interactions which are common between  $p^\uparrow Al$  and  $p^\uparrow Au$  collisions.

## VI. CONCLUSIONS

It is demonstrated that ultraperipheral  $p^\uparrow A$  collisions have large  $A_N$  for forward neutrons using the MC simu-

lation framework developed for this study. The present UPC simulation comprised the following two parts; first, the simulation of the virtual photon flux was performed by the STARLIGHT event generator and, second, the simulation of the  $\gamma^* p^\uparrow \rightarrow \pi^+ n$  interaction followed the differential cross sections predicted by MAID2007 unitary isobar model. In the  $\gamma^* p^\uparrow$  interaction, the target asymmetry  $T(\theta_\pi)$  was appropriately treated. According to the MC simulations, we found UPCs in  $p^\uparrow A$  collisions leading to  $A_N^{\text{UPC}(pA)} = 0.36$ . Concerning forward neutron production of  $p^\uparrow A$  hadronic interaction, the simulation model used an one-pion exchange model and the Glauber model. The single spin asymmetry was effectively taken in account by multiplying  $d\sigma_{pA \rightarrow nX}/d\Omega_n$  with  $1 + \cos \Phi A_N^{\text{HAD}(pA)}$  where  $A_N^{\text{HAD}(pA)} = -0.05$ . Combining the differential cross sections of UPCs and hadronic interactions, we simulated the  $x_F$  and  $\Phi$  distributions for inclusive forward neutrons. The  $A_N$  values



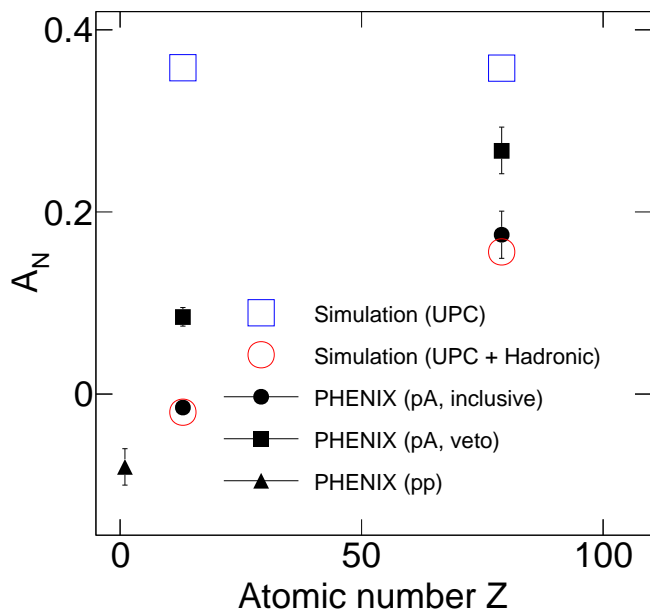


FIG. 5. Transverse single spin asymmetry  $A_N$  of forward neutron. Filled black marker indicates the PHENIX results. Open [red] circle and open [blue] squares indicate the asymmetry obtained by the sum of UPCs and hadronic interactions and by only hadronic interactions, respectively.

for inclusive neutrons at  $6.8 < \eta < 8.8$  and  $x_F > 0.4$  were predicted as  $-0.02$  and  $0.16$  in  $p^\dagger\text{Al}$  and  $p^\dagger\text{Au}$  collisions, respectively. These were consistent with the recently reported PHENIX results. The PHENIX data with the BBC veto in  $p^\dagger A$  collisions had larger  $A_N$  than the inclusive PHENIX data, but were smaller than  $A_N^{\text{UPC}}$ . This indicated that requiring the BBC veto enhanced the fraction of UPCs in the PHENIX data at a certain level, although the actual fraction was presently unreported.

For future analyses, we plan to extend the present simulation framework to include the contribution of the two-pion production  $\gamma^* p^\dagger \rightarrow \pi^+ \pi^0 n$ . This would provide a more accurate description of  $A_N$  of forward neutrons. Another extension would be to investigate the possible interference between electromagnetic and hadronic interactions, which is known as Coulomb-nuclear interference.

## ACKNOWLEDGMENTS

The author appreciates fruitful discussions with Y. Akiba, Y. Goto and I. Nakagawa.

- 
- [1] I. Nakagawa *et al.*, (PHENIX Collaboration), The First Transverse Single Spin Measurement in High Energy Polarized Proton-Nucleus Collision at the PHENIX experiment at RHIC, J. of Phys. Conf. Ser. **736**, 012017 (2016).
  - [2] A. Adare *et al.*, (PHENIX Collaboration), Inclusive cross section and single transverse spin asymmetry for very forward neutron production in polarized  $p+p$  collisions at  $\sqrt{s} = 200$  GeV, Phys. Rev. D **88**, 032006 (2013).
  - [3] C. Adler *et al.*, The RHIC zero degree calorimeters, Nucl. Instrum. Meth. **A 470** (2001) 488.
  - [4] B. Z. Kopeliovich, I. K. Potashnikova, and Iván Schmidt, Single transverse spin asymmetry of forward neutrons, Phys. Rev. D **84**, 114012 (2011).
  - [5] B. Z. Kopeliovich, I. K. Potashnikova, and Iván Schmidt, Leading Neutrons From Polarized Proton-Nucleus Collisions, arXiv:1611.07365.
  - [6] C. A. Bertulani and G. Baur, Electromagnetic processes in relativistic heavy ion collisions, Phys. Rep. **163** (1988) 299.
  - [7] C. A. Bertulani, S. R. Klein, and J. Nystrand, Physics of Ultra-Peripheral Nuclear Collisions, Ann. Rev. Nucl. Part. Sci. **55** (2005) 271.
  - [8] G. Mutsuka, Forward hadron production in ultra-peripheral proton-heavy-ion collisions at the LHC and RHIC, Eur. Phys. J. C **75**, 614 (2015).
  - [9] S. R. Klein, J. Nystrand, J. Seger, Y. Gorbunov, and J. Butterworth, STARlight: A Monte Carlo simulation program for ultra-peripheral collisions of relativistic ions, Comput. Phys. Comm. **212** (2017) 258.
  - [10] STARLIGHT webpage, <https://starlight.hepforge.org/>.
  - [11] D. Drechsel, S. S. Kamalov, and L. Tiator, Unitary isobar model –MAID2007, Eur. Phys. J. A **34**, 64.
  - [12] C. von Weizsäcker, Radiation emitted in collisions of very fast electrons, Z. Physik **88** (1934) 612.
  - [13] E. J. Williams, Nature of the high-energy particles of penetrating radiation and status of ionization and radiation formulae, Phys. Rev. **45** (1934) 729.
  - [14] D. Drechsel and L. Tiator, Threshold pion photoproduction on nucleons, J. Phys. G: Nucl. Phys. **18**, 449 (1992).
  - [15] W. Flauger and F. Mönig, Measurement of inclusive zero-angle neutron spectra at the CERN ISR, Nucl. Phys. B **109**, (1976) 347.
  - [16] S. Chekanov *et al.*, (ZEUS Collaboration), Study of the pion trajectory in the photoproduction of leading neutrons at HERA, Phys. Lett. B **610** 199 (2005).
  - [17] V. N. Gribov, Interaction of gamma quanta and electrons with nuclei at high-energies, Sov. Phys. JETP **30** (1970) 709.
  - [18] R. J. Glauber and G. Matthiae, High-energy scattering of protons by nuclei, Nucl. Phys. B **21** (1970) 135.
  - [19] V. Guzey and M. Strikman, Protonnucleus scattering and cross section fluctuations at RHIC and LHC, Phys. Lett. B **633** (2006) 245.
  - [20] B. Z. Kopeliovich, I. K. Potashnikova, Ivan Schmidt, and J. Soffer, Damping of forward neutrons in  $p+p$  collisions, Phys. Rev. D **78**, 014031 (2008).
  - [21] F.D. Aaron *et al.*, (H1 Collaboration), Measurement of leading neutron production in deep-inelastic scattering at HERA, Eur. Phys. J. C **68** (2010) 381.
  - [22] K. A. Olive *et al.* (Particle Data Group), Chin. Phys. C **38** (2014) 090001.



- [23] S. Chekanov *et al.*, (ZEUS Collaboration), Leading neutron production in  $e^+p$  collisions at HERA, Nucl. Phys. B **637**, 3 (2002).
- [24] A. Fix and H. Arenhövel, Double pion photoproduction on nucleon and deuteron, Eur. Phys. J. A **25**, 115 (2005).
- [25] M. Allen *et al.*, PHENIX inner detectors, Nucl. Instrum. Meth. A **499** (2003) 549.